Finite-Element Analysis of Lamb Wave Propagation in a Thin Aluminum Plate

SeJin Han[1]; Anthony N. Palazotto, F.ASCE[2]; and Charles L. Leakeas[3]

Abstract: Structural health monitoring (SHM) is an emerging technology that can be used to identify, locate, and quantify structural damages before failure. Among SHM techniques, Lamb waves are widely used since they can cover large areas from a single location. The development of various structural simulation programs has lead to increasing interest in whether SHM data obtained from the simulation can be verified by experimentation. The objective of this research is to determine the Lamb wave responses of SHM models using the finite-element software package ABAQUS CAE as a computational tool for an isotropic plate. These results are compared to experimental results and theoretical predictions under isothermal and thermal gradient conditions to assess the sensitivity of piezoelectric generated Lamb wave propagation. Simulations of isothermal tests are conducted over a temperature range of 0–190°F using 100 and 300 kHz as excitation frequencies. The changes in temperature-dependent material properties are used to measure the differences in the response signal's waveform and propagation speed. An analysis of the simulated signal response data demonstrated that elevated temperatures delay the Lamb wave propagation, although the delays are found to be minimal at the temperatures tested.

DOI: 10.1061/(ASCE)0893-1321(2009)22:2(185)

CE Database subject headings: Wave propagation; Finite element method; Aluminum; Plates; Structural reliability.

Introduction

Structural health monitoring (SHM) is an emerging technology that can be used to identify, locate, and quantify damage in a structural member or system before failure occurs. SHM addresses the urgent need to monitor the aging commercial and military aircraft infrastructure in the United States. The United States spends billions of dollars annually on the maintenance of plant equipment and facilities. Maintenance and repairs represent about a quarter of the commercial aircraft operating costs. Much of the civilian and military aircraft fleets have exceeded their design life while some of National Aeronautics Space Administration's space shuttles are more than 20 years old. The mounting costs of maintaining the aging infrastructure can be addressed through SHM systems that reduce scheduled and unscheduled repairs while increasing the safety and reliability of existing aircraft (Giurgiutiu 2005). Therefore, by using SHM techniques we have the benefit of reducing cost, increasing availability, and maintaining the safety of current and future air vehicle systems (Olson et al. 2006). Active SHM systems using interrogative Lamb waves are able to cover large areas from a single location making such systems cost effective and efficient. Another advantage is that Lamb waves provide through-the-thickness interrogation which allows detection of internal defects in thin materials (Wait et al. 2005). However, there are several disadvantages to using Lamb waves in SHM. These disadvantages are generally due to wave behavior and include the dispersive characteristics of Lamb waves and the existence of multiple waveforms in single frequency waves (Olson et al. 2006). Lamb waves, also known as guided waves, are a type of ultrasonic wave that remains guided between two free parallel surfaces such as the surfaces of a plate or shell structure (Mal 2004).

Elastic waves are a primary method of defect detection implemented in the field of SHM. These waves occur as a result of the restoring forces between particles when the material is elastically displaced. When elastic waves are excited in a medium, they transmit changes in stress and velocity inside the material (Lempriere 2002). This change in stress and velocity influences the quantitative wave characteristics such as the frequency, period, phase, wavelength, wave speed, wave number, and amplitude. Elastic waves consist of either bulk waves or guided waves. Bulk waves travel within the interior of a material away from any boundaries and exhibit a finite number of wave modes. However, guided waves travel on the surface of a material or through the thickness of thin materials and exhibit an infinite number of wave modes because the waves are dispersive (i.e., the wave speed is a function of frequency). These waves obey the same set of governing equations except that the guided waves are affected by the boundary conditions of the structure. Guided waves consist of Rayleigh or Lamb waves. These waves are generated from the coupling between longitudinal and vertical shear waves that are reflected and refracted at the free surfaces of a material. Rayleigh waves are free waves on the surface of a semi-infinite solid, so here the traction forces must vanish on the surface while the wave amplitude decays into the depth of the solid. Lamb waves are waves of plane strain that occur in a free plate. The traction forces must vanish on both the upper and lower surfaces of the plate. Due to these different characteristics, Rayleigh waves are useful for the damage detection of surface cracks in thick structures

[1]Graduate Student, Dept. of Aeronautics and Astronautics, Air Force Institute of Technology, Wright-Paterson AFB, OH 45433.

[2]Professor of Aerospace Engineering, Dept. of Aeronautics and Astronautics, Air Force Institute of Technology, Wright-Paterson AFB, OH 45433 (corresponding author). E-mail: anthony.palazotto@afit.edu

[3]Research Engineer, Dept. of Aeronautics and Astronautics, Air Force Institute of Technology, Wright-Paterson AFB, OH 45433.

Note. Discussion open until September 1, 2009. Separate discussions must be submitted for individual papers. The manuscript for this paper was submitted for review and possible publication on September 21, 2007; approved on October 22, 2007. This paper is part of the ***Journal of Aerospace Engineering***, Vol. 22, No. 2, April 1, 2009. ©ASCE, ISSN 0893-1321/2009/2-185–197/$25.00.

while Lamb waves are useful for the damage detection in plate and shell structures (Rose 1999).

One can classify two types of SHM techniques as "active" and "passive." The active technique uses sensors to interrogate the structure in order to detect damage presence, extent, and intensity. Active sensors act upon the structure in much the same way that conventional nondestructive evaluation (NDE) transducers do. Active sensors interact directly with the structure to find its state of health and reliability. However, passive SHM infers the state of the structure (i.e., loading, stress, environmental conditions, performance indicators, acoustic emissions from cracks, etc.) using passive sensors that are monitored over time and fed back into a structural model. Passive SHM only "listens" to the structure but does not interact with it (Giurgiutiu 2005). In this investigation the active SHM technique is used. An actuator is used to excite the structure while a sensor is used to monitor, collect, and process the response in an effort to provide a prognosis of the condition of the structure.

Ultrasonic Lamb wave NDE techniques are based on the propagation and reflection of elastic waves, with the assumption that damage in the structure alters the behavior of the waves. Typical ultrasonic methods include pitch-catch and pulse-echo techniques. When using the pitch-catch techniques, elastic waves are generated using an actuating transducer at one location on the structure, while the response is recorded using a sensing transducer at a different location. Damage is detected by examining the response at the sensing transducer. The severity of the damage is estimated based on the wave attenuation or dispersion. However, to locate the damage, various pairs of pitch-catch transducers are required. When using the pulse-echo techniques, the same transducer used to create the elastic waves is used to measure the response after the transducer has excited the structure. Damage is detected by investigating the echoes in the measured response due to wave reflections off damaged regions. The signal time of flight (TOF) can be used to locate the damage and quantify the amplitude of the reflected signal so as to assess the severity of the damage (Olson et al. 2006). A global vibration approach can be used to determine the location and nature of a defect in the structure by detecting a difference in the dynamical behavior of the structure. Changes in the frequency response functions (FRF) of a structure indicate the presence of damage. However, when the defects are small compared to the dimensions of the structure, it is not easy to distinguish the differences in the vibration response. Techniques have been developed to amplify the differences and eliminate noise which increases the effectiveness of using the vibration approach in detecting small defects in complex structures. The vibration approach is also used to detect widespread or extensive damage to a structure (Mal 2004). The wave propagation approach is a conventional NDE methodology that has long been used to detect and characterize damage. Unlike the vibration approach, the wave approach is used to detect and characterize small and hidden defects since the wave length is smaller than the defects that are found in the structure (Mal 2004).

Lamb wave theory was first introduced by Horace Lamb (Lamb 1917) while the first use of Lamb waves in SHM was performed by Worlton (1957). Cawley and Alleyne (1996) found that Lamb waves can propagate long distances and are useful for the inspection of large areas. They found that to apply this method successfully, the proper excitation of a single mode at a frequency located in a near nondispersive region is needed. Lowe et al. (1998) investigated the sensitivity of Lamb waves for defects. They also tried to relate proper wave modes to the defect size and strength of wave reflections. Ghosh et al. (1998) tried to find efficient Lamb modes for particular types of material defects. They propagated Lamb waves in large plates and computed the stress fields inside the plate. Derriso et al. (2005) studied simple Lamb wave propagation. In their study piezoelectric transducers are used as both actuator and sensor. Knowing the propagation distance of Lamb waves and the TOF, the group velocities of the signal received were calculated and experimental group velocity dispersion curves were generated and compared to theoretical group velocity dispersion curves (Derriso et al. 2005). Kundu et al. (1996) used Lamb waves for scanning internal defects for composite materials. In their investigation, the pitch-catch technique is used in an immersed actuator and sensor arrangement. Their scanning technique is effective in detecting internal defects such as missing fibers and fiber breakage (Kundu et al. 1996). Kundu et al. (1998) also studied the effectiveness of using Lamb waves for the detection of kissing bonds. The kissing bonds are defined as closed cracks under compressive normal stresses. They used a 1 Å wavelength Lamb wave with an asymmetric mode which proved to be sensitive to excitations in the interface crack surfaces. Grisso (2004) simulated the effects of a varying temperature on damage detection under the impedance-based SHM approach. Different temperatures change the material properties including the modulus of elasticity and density. Since the wave speed, which is used to determine the location of the defects, depends on the properties, different temperatures affect the local structural defects. In their study, the elastic modulus seemed to be significant for changing the wave speed; on the other hand, density was not significant.

In this investigation, piezoelectric transducers are used for both actuating and sensing Lamb waves. Thin disks made from ceramic material called piezoceramic lead zirconate titanate (PZT) are used as piezoelectric transducers. When transducers are attached to a test specimen for SHM, a transducer that sends out a wave is commonly referred to as an actuator, while a transducer that receives a wave is referred to as a sensor. Piezoelectric transducers are polarized such that a voltage differential applied across the thickness of the disk causes the radius of the disk to contract or expand. The radial displacement creates an elastic wave within the host material that propagates through a medium and eventually strains a sensor. A gain property relates strain to voltage, thus the resulting compression and expansion of the sensing transducer generates voltage differentials which are recorded as voltage amplitudes as a function of time (Andrews 2007).

Governing Equations for Lamb Wave Propagation

In order to be complete, the writers are presenting some of the basic theoretical relations that can capture the movement of a Lamb wave. A wave mode is defined as the manner of particle oscillation during wave propagation. In a solid material, particles can oscillate in four primary modes: (1) as longitudinal waves; (2) shear (transverse) waves; (3) surface waves; and (4) in thin materials as plate waves. These waves occur as a result of the material elastically displacing. Particles are displaced from their equilibrium positions and as a result internal (electrostatic) restoring forces between particles are combined with their inertia to generate oscillatory motions which can also be referred to as elastic waves. When shear waves occur, a structure's particles can move in two directions, both of which are perpendicular to the line of propagation. One wave can occur within the plane of the plate, horizontal shear waves, and vertical shear waves can propagate normal to the plate (through the thickness). In contrast, lon-

J. Aerosp. Eng., 2009, 22(2): 185-197

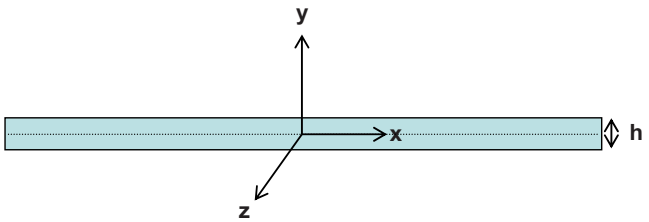

Fig. 1. Free plate geometry

gitudinal waves oscillate in the direction of wave propagation. In this investigation, plate waves are used in the experiments. Plate waves are "complex vibrational waves that travel through the entire thickness of a material" and are commonly referred to as guided Lamb waves. These waves result from the conversion between transverse (T) and longitudinal (L) modes (Andrews 2007).

Since Lamb waves are waves of plane strain that occur in a free plate, only displacements through the thickness (y direction) and in the direction of wave propagation (x direction) are taken into consideration (see Fig. 1). Displacements in the x direction correspond to longitudinal waves and displacements in the y direction correspond to vertical shear waves. If the z direction is considered in Lamb wave propagation, the resulting waves in this direction will be referred to as horizontal shear waves. Similar to vertical shear waves, horizontal shear waves propagate perpendicularly to longitudinal waves (Andrews 2007). Fig. 1 depicts particle motion in transverse and longitudinal waves. The black lines are the direction of particle motion and the red arrows are the direction of wave propagation (Andrews 2007). Fig. 2 depicts particle motion in transverse and longitudinal waves.

Wave propagation is dependent on the density ρ and elastic properties of a medium. The longitudinal wave speed is characterized by the Young's modulus (E) as (Andrews 2007)

$$c_L = \sqrt{\frac{E}{\rho}} \tag{1}$$

Similarly, the transverse (shear) wave speed is characterized by the shear modulus (G) as (Andrews 2007)

$$c_T = \sqrt{\frac{G}{\rho}} \tag{2}$$

Since the modulus values for an isotropic material are constant in all directions the previous longitudinal and transverse wave speed equations can be replaced with the Lamé constants (λ and μ). Additionally, the modulus originally used for the longitudinal wave speeds has been modified. When the lateral dimension of a medium, that is, of the wave propagating direction, is much greater than the wavelength of the wave traveling through it the modulus is sometimes referred to as the plane wave modulus (Timoshenko and Goodier 1970). The plane wave modulus

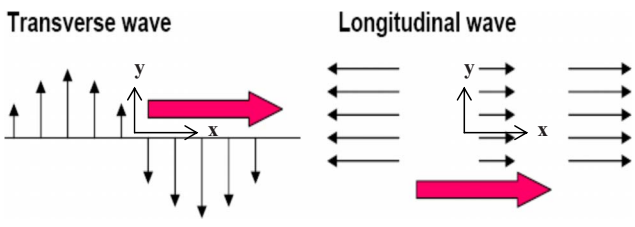

Fig. 2. Transverse and longitudinal waves

is equivalent to $\lambda+2\mu$ and the shear modulus is equivalent to μ (Saada 1993). The new equations for the longitudinal and transverse wave speeds, along with the plane wave modulus, are (Timoshenko and Goodier 1970)

$$c_L = \sqrt{\frac{\lambda + 2\mu}{\rho}} \tag{3}$$

$$c_T = \sqrt{\frac{\mu}{\rho}} \tag{4}$$

Recall that as guided waves, Lamb waves are dispersive. At this point, the longitudinal and transverse waves are nondispersive since their wave speeds are only a function of material properties and not frequency. The dispersive equations, also known as the Rayleigh–Lamb frequency equations, are introduced subsequently.

The equations of motion can be derived from the basic elasticity equations consisting of the three equations of motion, six independent strain-displacement equations, and six independent constitutive equations, assuming isotropic material properties. They are shown using Cartesian tensor notation, and one can find a completely developed form of these equations in Rose (1999). The work presented here is a partial reproduction of these equations for completeness

$$\mu u_{i,jj} + (\lambda + \mu) u_{j,ji} + \rho f_i = \rho \ddot{u}_i \tag{5}$$

where the Lame' constants=μ and λ; u=displacement; and f =applied force. Additionally, the subscripts i and j equal x, y, or z. The free plate problem is governed by the equations of motion, as indicated in Eq. (5), and requires the surface traction boundary conditions (Rose 1999)

$$t_i = \sigma_{ji} n_j \tag{6}$$

The three traction components t_i are prescribed on the boundary with a unit normal n (Achenbach 1980). A free plate surface is considered traction free.

When solving for the free plate problem using the method of potentials, the Helmholtz decomposition of the displacement vector can be used in the form (Achenbach 1980)

$$u = \nabla\phi + \nabla \times \psi \tag{7}$$

where u=displacement vector, φ=scalar potential; and ψ =vector potential. For a plane strain problem, the following conditions hold (Achenbach 1980):

$$u_z = w \equiv 0, \quad \frac{\partial}{\partial z}(\,) \equiv 0 \tag{8}$$

The components of the displacement vector become

$$u_x = \frac{\partial \phi}{\partial x} + \frac{\partial \psi}{\partial y} \tag{9}$$

$$u_y = \frac{\partial \phi}{\partial y} - \frac{\partial \psi}{\partial x} \tag{10}$$

The equation of motion can now be written as

$$\nabla[(\lambda + 2\mu)\nabla^2\phi - \rho\ddot{\phi}] + \nabla \times [\mu\nabla^2\psi - \rho\ddot{\psi}] = 0 \tag{11}$$

Setting the terms in each bracket to zero and simplifying, the equations of motion for the longitudinal and shear waves become (Rose 1999)

J. Aerosp. Eng., 2009, 22(2): 185-197

$$\frac{\partial^2 \phi}{\partial x^2} + \frac{\partial^2 \phi}{\partial y^2} = \frac{1}{c_L^2}\frac{\partial^2 \phi}{\partial t^2} \tag{12}$$

$$\frac{\partial^2 \psi}{\partial x^2} + \frac{\partial^2 \psi}{\partial y^2} = \frac{1}{c_T^2}\frac{\partial^2 \psi}{\partial t^2} \tag{13}$$

where c_L and c_T=longitudinal and transverse wave speeds in the material, respectively. The time dependent solutions to Eqs. (12) and (13) are harmonic and thus have the form

$$\phi = \Phi(y)\exp[i(kx - \omega t)] \tag{14}$$

$$\psi = \Psi(y)\exp[i(kx - \omega t)] \tag{15}$$

where ω=circular frequency of the external pulse applied to the surface; and k=parameter to be determined, called the wave number, numerically equal to ω/c_p, where c_p=phase velocity to be discussed subsequently. These solutions represent traveling waves in the x direction and standing waves in the y direction. This is evident from the fact that there is only an unknown "static" function for the y dependence. The substitution of Eqs. (14) and (15) into the equations of motion Eqs. (12) and (13) yields solutions governing the unknown functions Φ and Ψ. The solutions to these equations are (Rose 1999)

$$\Phi(y) = A_1 \sin(py) + A_2 \cos(py) \tag{16}$$

$$\Psi(y) = B_1 \sin(qy) + B_2 \sin(qy) \tag{17}$$

The unknown amplitude constants A and B are determined from the boundary conditions of the problem and are associated with the longitudinal and shear waves, while the subscripts 1 and 2 indicate the propagation direction as outward and inward directions to the plate surface, respectively.

Since the field variables involve sines and cosines with the variable y, which are odd (or even for cosines) functions about $y=0$, the solution is split into two sets of modes (i.e., symmetric and asymmetric modes). Specifically, for displacement in the x direction, the motion will be symmetric with respect to the midplane of the plate if u_x contains cosines but will be asymmetric if u_x contains sines. The opposite is true for displacements in the y direction. Thus, the modes of wave propagation in the plate are split into two systems (Rose 1999):

Symmetric modes

$$\Phi = A_2 \cos(py)$$

$$\Psi = B_1 \sin(qy)$$

$$u = u_x = ikA_2 \cos(py) + qB_1 \cos(qy)$$

$$v = u_y = -pA_2 \sin(py) - ikB_1 \sin(qy)$$

$$\sigma_{yx} = \mu[-2ikpA_2 \sin(py) + (k^2 - q^2)B_1 \sin(qy)]$$

$$\sigma_{yy} = -\lambda(k^2 + p^2)A_2 \cos(py) - 2\mu[p^2 A_2 \cos(py) + ikqB_1 \cos(qy)] \tag{18}$$

Asymmetric modes

$$\Phi = A_1 \sin(py)$$

$$\Psi = B_2 \cos(qy)$$

$$u = u_x = ikA_1 \sin(py) - qB_2 \sin(qy)$$

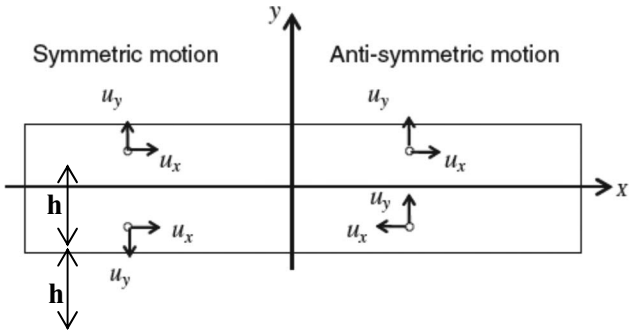

Fig. 3. Symmetric and asymmetric particle motion across plate thickness

$$v = u_y = pA_1 \cos(py) - ikB_2 \cos(qy)$$

$$\sigma_{yx} = \mu[2ikpA_1 \cos(py) + (k^2 - q^2)B_2 \cos(qy)]$$

$$\sigma_{yy} = -\lambda(k^2 + p^2)A_1 \sin(py) - 2\mu[p^2 A_1 \sin(py) - ikqB_2 \sin(qy)] \tag{19}$$

For the symmetric modes, the wave structure across the thickness of the plate is symmetric for u and asymmetric for v. On the other hand, for asymmetric modes, the wave structure across the thickness is symmetric for v and asymmetric for u. Fig. 3 shows the symmetric and asymmetric particle motion across the plate thickness.

The unknown constants A_1, A_2, B_1, and B_2 can be determined by applying the traction-free boundary condition for a free plate in the case of plane strain (Rose 1999)

$$\sigma_{yx} = \sigma_{yy} \equiv 0 \quad \text{at } y = \pm d/2 = \pm h \tag{20}$$

The resulting displacement, stress, and strain fields depend upon the type of mode. However, applying the boundary conditions will give a homogeneous system of two equations for the two appropriate constants A_2, B_1 for the symmetric case and A_1, B_2 for the asymmetric case. For homogeneous equations, the determinant of the coefficient matrix must vanish in order to ensure unique solutions other than the trivial one. Using Eq. (20) the following relations are found from computing the determinant of the coefficient matrices for both symmetric and asymmetric modes (Rose 1999):

$$\frac{\tan(qh)}{\tan(ph)} = -\frac{4k^2 pq}{(q^2 - k^2)^2} \quad \text{(symmetric modes)} \tag{21}$$

$$\frac{\tan(qh)}{\tan(ph)} = -\frac{(q^2 - k^2)^2}{4k^2 pq} \quad \text{(asymmetric modes)} \tag{22}$$

For a given ω and derived k, the displacements can be determined from Eqs. (18) and (19) and for both symmetric and asymmetric modes. Eqs. (21) and (22) are known as the Rayleigh–Lamb frequency relations, or dispersion relations, and can be used to determine the velocity at which a wave of a particular frequency will propagate within the plate. Since the Lamb waves are dispersive, the wave speed, or phase velocity, is a function of frequency. These individual waves interact and the resulting wave propagates at a group velocity which may be different from the individual phase velocities (Olson et al. 2006). Numerical methods for calculating phase and group velocity dispersion curves are outlined by Rose (1999) to solve Eqs. (21) and (22).

Phase Velocity (c_p) and Group Velocity (c_g)

In this section, the basic concept of the phase velocity and the group velocity is introduced. The phase velocity is the velocity at which a wave of a single frequency propagates. Since the period ($\tilde{T}$) of the signal is the time in which the signal travels the length of a single wave, the wavelength ($\tilde{\lambda}$) divided by the period will be the phase velocity (Lathi 2005)

$$c_p = \frac{\tilde{\lambda}}{\tilde{T}} \tag{23}$$

Since the frequency (f) is the number of repetitions of the signal per second, the period (repetition interval) can be expressed using the frequency (Lathi 2005)

$$\tilde{T} = \frac{1}{f} \tag{24}$$

Using Eq. (24), the phase velocity in Eq. (23) can be expressed as (Andrews 2007)

$$c_p = f\tilde{\lambda} \tag{25}$$

The circular frequency (ω) is expressed as (Lathi 2005)

$$\omega = 2\pi f \tag{26}$$

while the circular wave number (k) is expressed as (Andrews 2007)

$$k = \frac{2\pi}{\tilde{\lambda}} \tag{27}$$

Substituting the frequency (f) from Eq. (26) and the wavelength ($\tilde{\lambda}$) from Eq. (27) into Eq. (25) generates a new phase velocity equation as (Andrews 2007)

$$c_p = \frac{\omega}{k} \tag{28}$$

The group velocity is the propagation velocity of a wave packet. A wave packet is a group of waves that travel together with similar but distinct frequencies and varying wave speeds. As an example, consider an excitation signal that has energy over a range of frequencies. When this excitation pulse is transmitted in a specimen, the propagating wave is actually comprised of several component waves of varying frequencies and phase speeds. If these waves of varying phase speeds are superimposed then the speed of the resulting wave is the group velocity. The group velocity is also referred to as the signal velocity or the velocity at which the energy of a wave packet is conveyed through a structure (Andrews 2007). The group velocity can be defined using a classical approach. Consider a cosine wave with components that compose a wave packet (Rose 1999)

$$u = A\cos(k_i x - \omega_i t) \tag{29}$$

At some time increment, $t = t_0 + dt$ the changes in phase of any individual component can be represented as (Rose 1999)

$$dP_i = \{k_i(x_0 + dx) - \omega_i(t_0 + dt)\} - \{k_i x_0 - \omega_0 t\} = k_i dx - \omega_i dt \tag{30}$$

In order for the wave packet to be maintained, the change in phase for all components should be the same and thus one can write group velocity in terms of the phase velocity

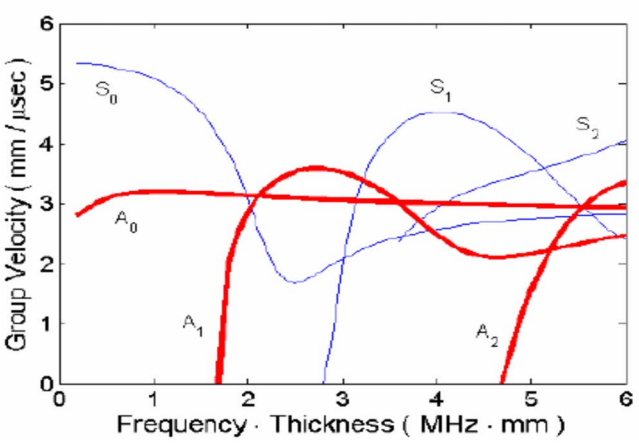

Fig. 4. Theoretical group velocity dispersion curves for aluminum plate

$$c_g = d\omega\left[d\left(\frac{\omega}{c_p}\right)\right]^{-1} = d\omega\left[\frac{d\omega}{c_p} - \omega\frac{dc_p}{c_p^2}\right]^{-1} = c_p^2\left[c_p - \omega\frac{dc_p}{d\omega}\right]^{-1} \tag{31}$$

where c_g=group velocity; ω=circular frequency; and k=circular wave number.

Using Eq. (26), the group velocity can be written as (Rose 1999)

$$c_g = c_p^2\left[c_p - (fd)\frac{dc_p}{d(fd)}\right]^{-1} \tag{32}$$

(The product fd is equal to the frequency times the plate thickness.)

When the phase velocity or wave speed is independent of frequency, the phase velocity is equivalent to the group velocity. However, in dispersive mediums the phase velocity is dependent on frequency. When the wave speed decreases with frequency, the group velocity is less than the phase velocity. Conversely, when the wave speed increases with frequency the group velocity is greater than the phase velocity. In a dispersive medium, a wave packet generally propagates at the group velocity which is slower than the phase speed of the original excitation signal (Andrews 2007).

Lamb Wave Modes

When a free plate is excited, the excitation will generate guided Lamb waves in the plate. The Lamb waves are composed of the coupling between the x and the y directed elastic displacements of particles. The x direction displacement of the particles is called the longitudinal wave and the y direction displacement of the particles is called the transverse wave. Since, for Lamb waves, the angular frequency is not directly proportional to the wave number, dispersion occurs and the waves become distorted as they propagate. Therefore, Lamb waves contain various wave modes. The wave modes can be categorized by two types [i.e., symmetric (S_i) and asymmetric (A_i) modes]. As shown in Fig. 3, the motion of the particles is symmetric to the midplane of the plate in symmetric wave modes, and conversely, motion of the particles is asymmetric to the midplane of the plate in asymmetric wave modes.

In the guided Lamb wave response received, multiple symmetric and asymmetric wave modes can coexist. The number of co-

J. Aerosp. Eng., 2009, 22(2): 185-197

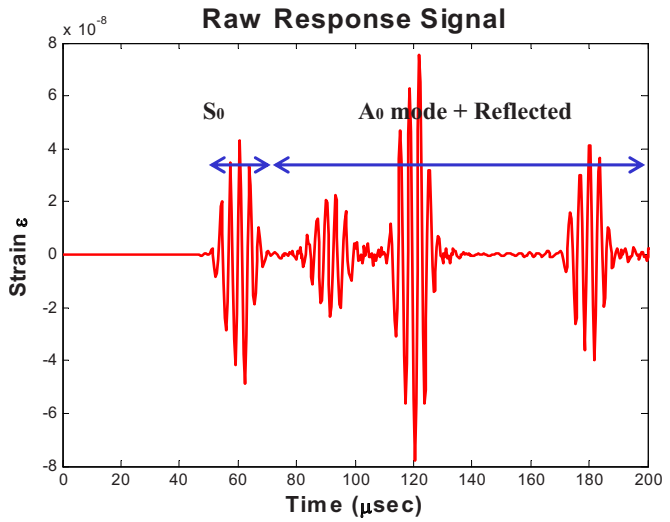

Fig. 5. Lamb wave modes of response

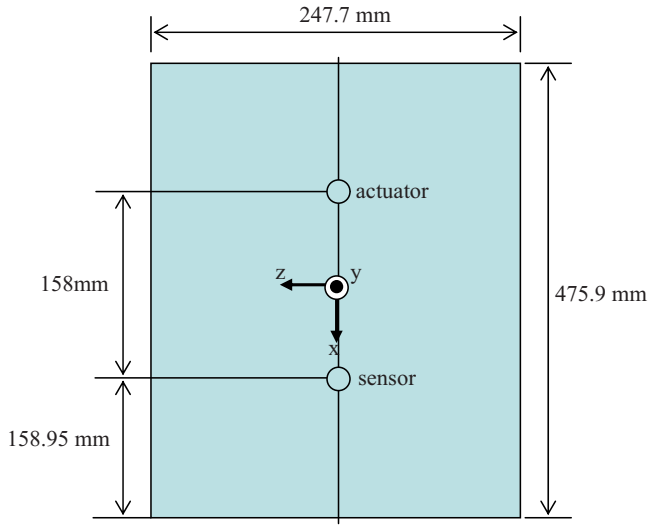

Fig. 6. Schematic of aluminum sheet specimen for isothermal testing

existing wave modes goes up as the frequency-thickness product increases, as seen in Fig. 4. Since the existence of many wave modes in the response makes the analysis difficult, isolating the fundamental modes (i.e., S_0 and A_0) from other wave modes (i.e., S_1, S_2, S_3, A_1, A_2, and A_3,…) is recommended. In order to trace a particular mode, wave mode isolation is very important when studying SHM. In this investigation, the frequency-thickness product (fd) will be kept below 1.8 MHz mm in order to isolate the group velocity of the S_0 mode. Since the group velocity of the S_0 mode is faster than the group velocity of the A_0 mode it becomes straightforward to study the S_0 mode. Isolating the A_0 mode can be difficult since the A_0 mode can be mixed with reflected waves as shown in Fig. 5. Thus, in this investigation the S_0 mode is analyzed in the response signal. The thickness of the specimen (free plate) and the frequency of the excitation signal are determined by the restriction of the frequency-thickness product (fd). Using frequencies under 500 kHz and a plate thickness of 1 and 0.6 mm satisfies the isolating criteria (i.e., $fd < 1.8$ MHz mm).

Model Development

Modeling of Specimen I

The study was carried out using the finite-element method (Moser et al. 1999) incorporating ABAQUS (2006). Fig. 6 shows a schematic of the aluminum sheet specimen used for the simulation of the isothermal test and Table 1 shows its dimensions. It is obvious that the thermal environment considering an isothermal condition affects the Young's modulus of aluminum as shown in Table 5. Piezoelectric transducers are used for both the actuator and sensor for the Lamb wave propagation study. These transducers are centered along the width of the plate and placed along the length. The length of the propagation distance allows time for changes in the signal to occur.

In order to use ABAQUS (2006), the specimen is converted to a two-dimensional (2D) plane strain model (z direction is infinite) as shown in Fig. 7. The ideal model for Lamb wave propagation is a thin plate with boundary conditions that eliminate wave reflection. Even though it is impossible to make such an ideal model in real life, our specimen is still adequate because it is sufficiently wide to get the S_0 response before any influences from the reflected wave occur.

Modeling of Specimen III

Fig. 8 and Table 2 show a schematic of the aluminum sheet specimen used for the simulation of the thermal gradient test with its dimensions. As shown in Timoshenko and Goodier (1970), a thermal gradient creates a through the thickness stress field. This stress field affects the wave speed of propagation. In the experiment, for producing a symmetric thermal gradient condition between the actuator and sensor, a 14 in. PROTHERM 40 series infrared heater is placed in the middle of the plate. For thermal gradient testing, a relatively large specimen, as compared to the isothermal test, is used. The use of the larger specimen assures that the transducers are close to room temperature while the center of the specimen is heated to temperatures exceeding 200°F. Additionally, the larger specimen also provides sufficient propagation distance making it easier to analyze the time delay due to the thermal gradient region. The three thermal gradient data (i.e., TG 1, TG 2, and TG 3) are captured using ten thermocouples in the experiment after an equilibrium condition is reached as shown in Table 3. The 2D temperature profile is shown in Fig. 9, while the specimen is converted to a 2D plane strain model (z direction is infinite) as shown in Fig. 10.

Material Properties of 2024-T3 Aluminum

The material properties of the two specimens used in this investigation are 2024-T3 aluminum which is an isotropic material. Table 4 shows unit conversions of 2024-T3 aluminum properties used in this study. The temperature dependent properties of the

Table 1. Dimension of Aluminum Sheet Specimen for Isothermal Testing

Specimen	Length (mm)	Width (mm)	Thickness (mm)	Propagation distance (mm)
I	475.9	247.7	1.015	158

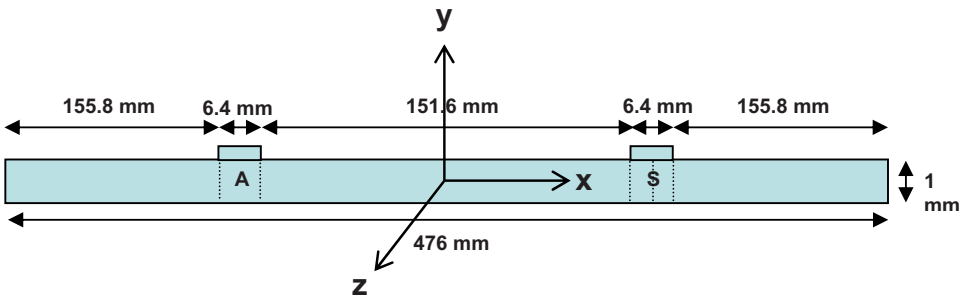

Fig. 7. Dimensions of Specimen I used for isothermal model showing locations of actuator and sensor

2024-T3 aluminum are given in Table 5 and shown in Fig. 11. These properties are taken from MIL-HDBK-5 (Department of Defense 2003).

Determining Element Edge Length (L_e) and Time Step (Δt) of FE Models

The lowest phase velocity (i.e., transverse wave speed), and hence the shortest wavelength sets the maximum permissible grid spacing that must be chosen so that spatial inaccuracies due to the finite-element (FE) discretization do not occur (Alleyne and Cawley 1991). The size of the elements is chosen in a manner so that the propagating waves are spatially resolved (Moser et al. 1999). To do this, more than 10 nodes per wavelength is adequate (Alleyne and Cawley 1991). A minimum element edge length of 0.1 mm and a time step of 5 ns are used in the FE model for this investigation (Han 2007).

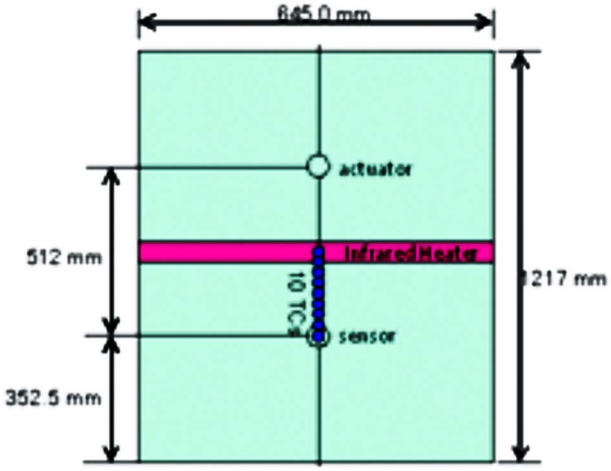

Fig. 8. Schematic of aluminum sheet specimen for thermal gradient testing

Table 2. Dimension of Aluminum Sheet Specimen for Thermal Gradient Testing

Specimen	Length (mm)	Width (mm)	Thickness (mm)	Propagation distance (mm)
III	1,217	645.0	0.6345	512

Five and a Half Cycle Hanning-Window Excitation Signal

The 5 1/2 cycle Hanning-window excitation signal is used in this study because it has a number of advantages. First, it reduces the energy at frequencies other than the excitation or "center" frequency. Second, since the signal is based on a limited cycle sinusoidal tone burst, the undesired reflections between packets are reduced, thereby allowing for time of arrival (TOA) calculations. Figs. 12 and 13 provide the 5 1/2 cycle Hanning-window excitation signals at 100 and 300 kHz. The addition of the half cycle, to an integer number of cycles, provides a distinct peak in the excitation signal and provides its symmetry. Since the frequency content is narrow relative to the center frequency this is considered a narrow-band signal. The simulation excitation signal is fed directly into the finite-element model as a forcing function while the theoretical excitation signal is substituted into Eqs. (18), (19), (21), and (22) incorporating the Rayleigh–Lamb wave relations previously discussed.

Convergence Study

A convergence study (Han 2007) is carried out to verify the modeling methods used in the FE model. A FE model using an element edge length (L_e) of 0.05 mm (one half of the original element edge length) is used with a 300 kHz excitation signal in Specimen I. The difference in amplitude between the two large

Table 3. Specimen III Thermal Gradient Profiles

		Thermocouple number									
		1	2	3	4	5	6	7	8	9	10
Location (mm)		0	24	47	77	106	136	166	196	226	256
Temp (°F)	RM						75				
	TG 1	281	220	148	123	107	98	91	88	75	75
	TG 2	239	189	142	122	107	99	91	89	75	75
	TG 3	184	153	123	110	100	96	89	88	75	75

J. Aerosp. Eng., 2009, 22(2): 185-197

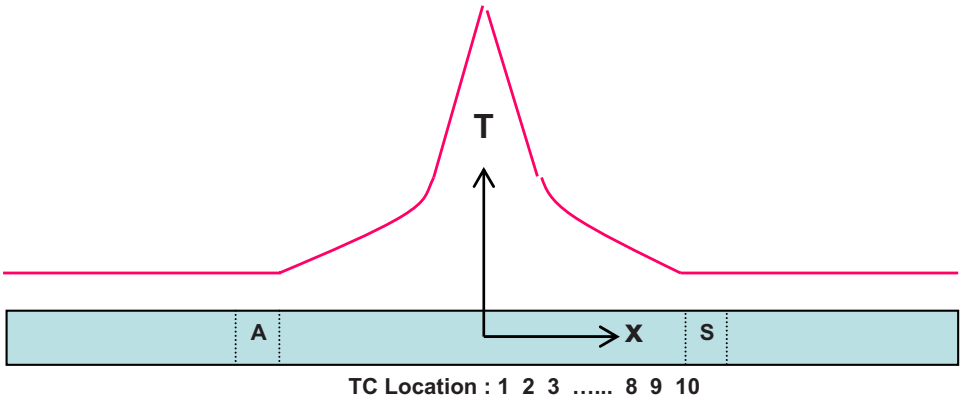

Fig. 9. Specimen III thermal gradient profiles using ten thermocouples

peaks, between the original and refined models, in the propagating wave, is calculated as 1.3%. Thus, the model chosen for all of the analysis is based on the model using the original element edge length and time step.

Discussion and Results

Isothermal Testing of the Specimen I

The isothermal condition is analyzed using Specimen I. The analysis focuses on the delayed TOA that is due to the elevated temperature and the TOA agreement between the simulated, theoretical, and experimental S_0 responses.

S_0 Response at 100 kHz

For this analysis, the 100 kHz excitation signal is used to generate a response. The S_0 response of the experiment in this low frequency is mixed with magnetic noise, so it is not possible to compare with other results. The magnetic noise is due to the induction between the wires transmitting the signals. Magnetic induction occurs when the magnetic field generated from a current in one wire generates an electric current in an adjacent wire. Since the wires are in close proximity to each other during testing, the magnetic field around the wire carrying the excitation signal transmits the same signal over to the receiving wire (Andrews 2007). The existence of magnetic induction can be seen in the raw signal at 300 kHz as shown in Fig. 14.

Therefore, in this section, two types of S_0 responses are compared under the 0, 25, 50, 75, 100, 125, 150, 175, and 190°F isothermal conditions. The first type of S_0 response is the finite-element result of an ABAQUS simulation. In this study, ABAQUS provides displacements of the three sensing points, thus a conversion from displacement to strain is conducted using Matlab. The second type of S_0 response is the theoretical response. Andrews (2007) and Air Force Research Laboratory (AFRL) provided the Matlab (MathWorks, Natick, Mass.) codes which can generate a theoretical excitation signal and S_0 response using Rayleigh–Lamb equations.

Fig. 15 shows typical waveform comparisons between two

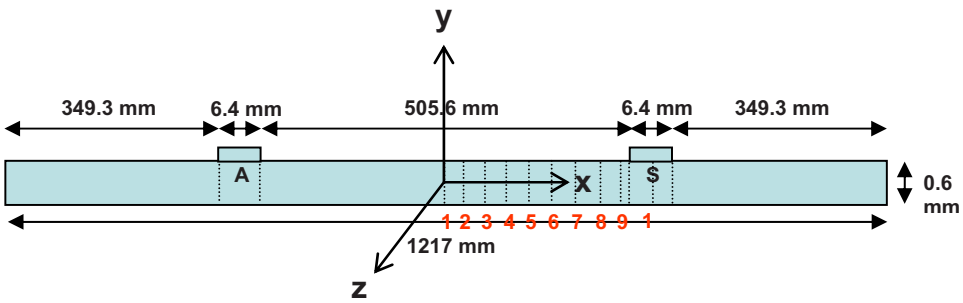

Fig. 10. Dimensions of Specimen I used for thermal gradient model showing locations of actuator and sensor

Table 4. Unit Conversions of Basic 2024-T3 Aluminum Properties

Elastic modulus(E)	E=68.95 GPa=68.95×10^9 N/m^2=68,947.6 N/mm^2=9.99×10^6 psi
Shear modulus (G)	G=25.92 GPa=25.92×10^9 N/m^2=25,920 N/mm^2
Poisson's ratio (ν)	ν=0.33
Density (ρ)	ρ=2.768 g/cm^3=2,767.8 kg/m^3=2.7678−9 N s^2/mm^4
Thermal conductivity($\tilde{k}$)	k=121 $w/m\cdot$° C=121 N m/s·m·° C=121 N/s·° C
Specific heat(C_P)	C_P=0.963 kJ/kg·° C=963 N·m/kg·° C=963E6 mm^2/s^2 ° C
Thermal expansion coefficient(α)	α=22.7E−6-1/° C

Table 5. Temperature Dependent Properties of 2024-T3 Aluminum

Temperature (T)		Young's modulus (E)		Poisson's ratio (ν)
(°F)	(°C)	(psi)	(N/mm^2)	
0.155642	−17.691310	10,173,528.9624726	70146.52293	0.33
20.0389	−6.645056	10,097,828.9624726	69624.57112	
45.6031	7.557278	10,072,528.9624726	69450.12752	
62.6459	17.025500	10,022,028.9624726	69101.92982	
84.6858	29.269889	99,82,728.96247261	68830.95616	
104.4110	40.228333	9,924,298.9624726	68428.08108	
124.1370	51.187222	9,880,458.96247261	68125.80410	
145.5060	63.058889	9,79,2778.96247261	67521.25015	
163.5880	73.104444	9,734,318.96247261	67118.16822	
183.3130	84.062778	9,646,638.96247261	66513.61427	
203.0390	95.021667	9,558,958.96247261	65909.06032	
222.7640	105.980000	9,471,278.96247261	65304.50637	
244.1330	117.851667	9,354,368.96247261	64498.41145	
263.8590	128.810556	9,237,458.96247261	63692.31653	
283.5840	139.768889	9,091,318.9624726	62684.68064	
303.3100	150.727778	8,959,798.9624726	61777.84972	
323.0350	161.686111	8,828,268.96247261	60870.94984	
341.1170	171.731667	8,667,518.96247261	59762.57795	
360.8420	182.690000	8,492,158.96247261	58553.47005	
382.2120	194.562222	8,287,558.96247261	57142.75223	
403.5810	206.433889	8,068,358.9624726	55631.36735	
423.3060	217.392222	7,849,148.96247261	54119.91352	
443.0320	228.351111	7,586,098.96247261	52306.18272	
462.7570	239.309444	7,323,058.9624726	50492.52086	
484.1260	251.181111	7,060,008.9624726	48678.79006	
502.2080	261.226667	6,767,738.96247261	46663.58724	
525.2210	274.011667	6,417,008.96247261	44245.30249	
544.9470	284.970556	6,051,658.96247261	41726.21277	
563.0280	295.015556	5,715,548.96247261	39408.73298	
584.3980	306.887778	5,335,588.96247261	36788.90726	
602.4790	316.932778	4,999,468.96247261	34471.35851	

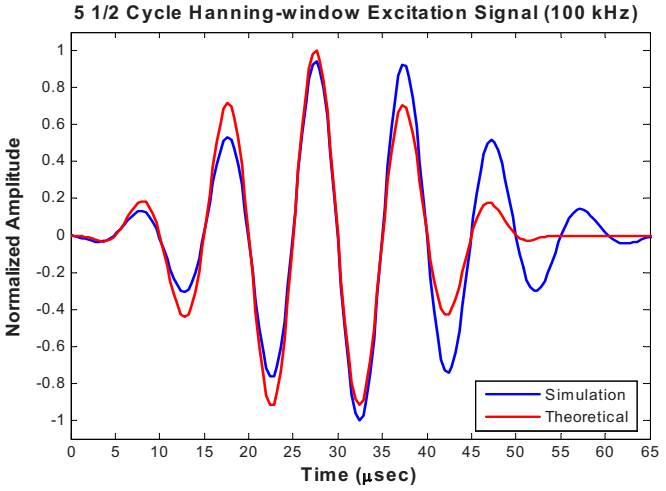

Fig. 12. 5 1/2 cycle Hanning-window excitation signals at 100 kHz

types of S_0 response for specific steps of the temperature condition. Table 6 shows TOA differences between two types of S_0 responses. The TOA is calculated by measuring the peak amplitude time of the S_0 response. However, visual modification is needed since the entire peak doesn't appear in the middle of the waves. In the cases of the 100 and 125°F temperatures, the peak amplitudes do not appear in the middle of the simulated responses; they are located at a distance forward from the middle. In these cases, the midwave amplitude is the criteria for TOA calculation even though its amplitude is not the largest. In order to reduce the complexity when deciding on the criteria of the waves, a reading technique from the back to the front in the wave is recommended.

Before the waveform and the TOA are compared, each S_0 response is normalized with respect to its absolute maximum amplitude and the time delay between simulated and theoretical excitation signals are considered for plotting and TOA calculations. Four conclusions are drawn from the results. First, the theoretical S_0 responses are a little faster than the simulated S_0 responses. Second, as the temperature is increased the two types

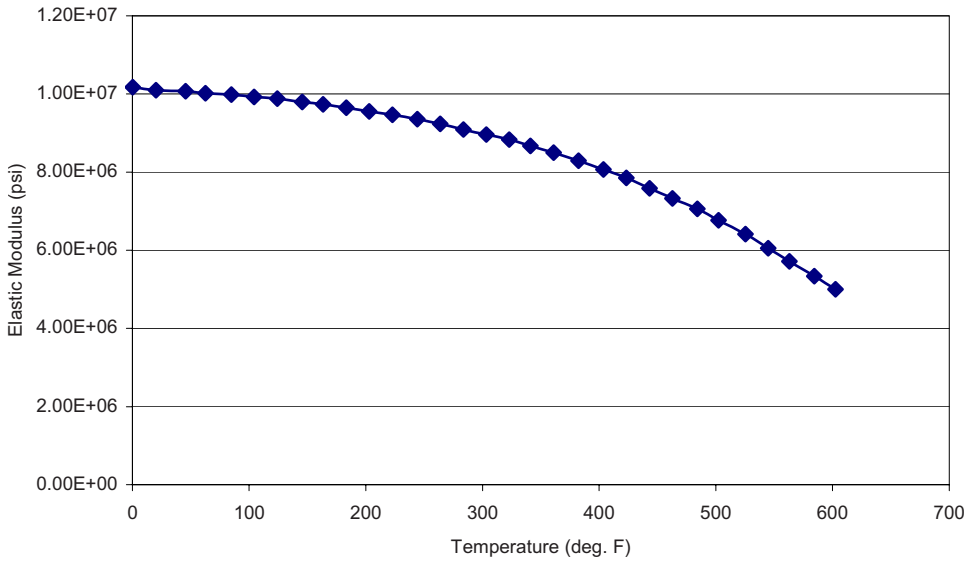

Fig. 11. Aluminum modulus of elasticity varying with temperature

J. Aerosp. Eng., 2009, 22(2): 185-197

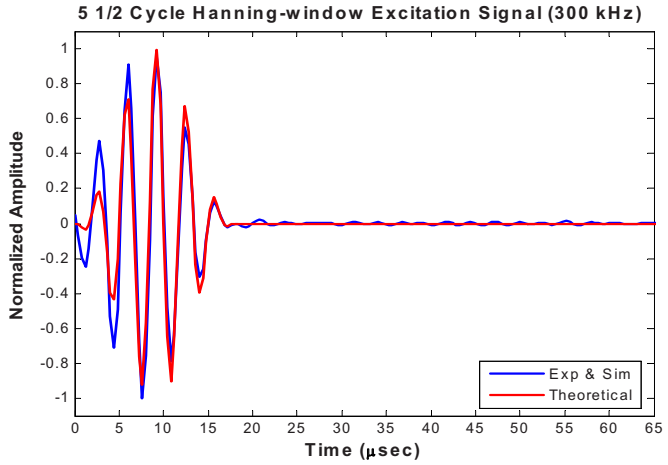

Fig. 13. 5 1/2 cycle Hanning-window excitation signals at 300 kHz

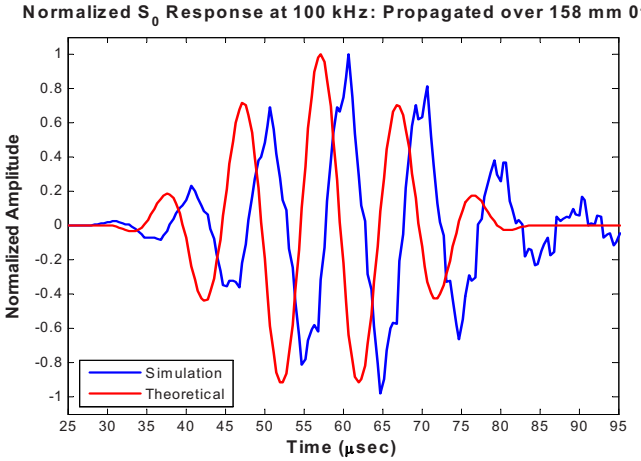

Fig. 15. Specimen I S_0 response at 100 kHz (0°F)

of S_0 responses are delayed by a small amount of time. The second phenomenon is related to the delayed TOA due to the elevated temperature. Third, some fluctuations in the simulated responses can be observed at around 80–95 μs. These are explained by the differences between the simulated excitation signal and the theoretical excitation signal. As shown in Figs. 12 and 13, each simulated excitation has some noise after its 5 1/2 cycle Hanning-windowed signal is completed. This noise can affect the response of the signal. Fourth, the most important reason that causes the differences between the theoretical S_0 and the simulated S_0 response is the different types of analysis performed between ABAQUS and Matlab. ABAQUS simulates the actual wave traveling, thus the wave in the simulated response is the wave packet that is generated by interaction between component waves during propagation. However, Matlab does not carry out actual wave propagation analysis, it only shows the same waveform as the excitation signal at the response. This is the reason there is no fluctuation in the theoretical response.

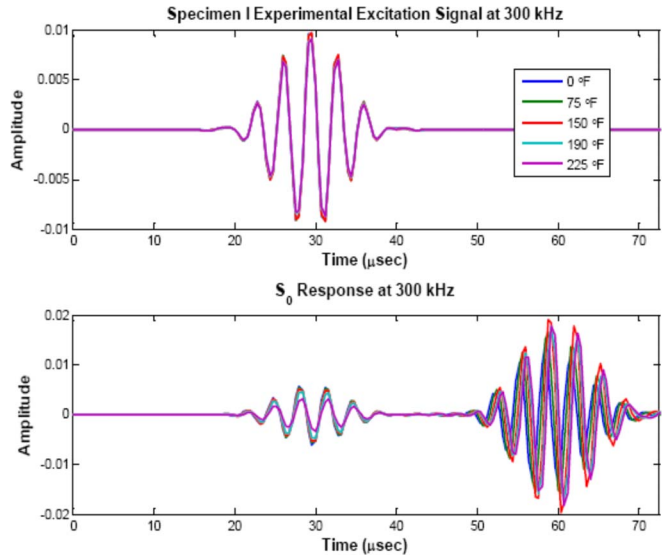

Fig. 14. Existence of magnetic noise

S_0 Response at 300 kHz

In this section, the experimentation (Andrews 2007) is carried out with respect to the S_0 responses and compared under the 0, 50, 100, 125, 150, 175, and 190°F isothermal conditions using the 300 kHz excitation signal.

Fig. 16 shows a typical visual waveform comparison between the three types of S_0 response for several steps of the temperature condition. Table 7 shows TOA differences between the three types of S_0 responses. Before comparison of the waveform and the TOA, each of the three types of S_0 response is normalized with respect to its own absolute maximum amplitude and the time delay between simulated, theoretical, and experimental excitation signals is plotted. As previously discussed, the theoretical S_0 responses are a little bit faster than the experimental S_0 responses while the experimental S_0 responses are little bit faster than the simulated S_0 responses. In addition, as anticipated, the three types of S_0 responses are delayed by a small amount of time as the temperature is increased.

In addition, some small and large fluctuations in experimental responses are observed before and after the S_0 responses. These can be explained by two factors. The first is the difference between the simulated/experiment (they use the same excitation) excitation signal and the theoretical excitation signal. As previously discussed, the noise contained in the excitation signal could affect the response. However, the first factor is not sufficient to explain the existence of the small fluctuations before the S_0 re-

Table 6. Specimen I TOA of S_0 Response at 100 kHz

	Time of arrival (TOA)		TOA difference
Temperature (°F)	Simulation TOA (μs)	Theoretical TOA (μs)	SIM—THEO (μs)
0	59.2	57.2	2.0
25	59.2	57.2	2.0
50	60.8	57.2	3.6
75	60.8	57.2	3.6
100	60.8	57.6	3.2
125	61.2	57.6	3.6
150	61.2	57.6	3.6
175	61.6	58.0	3.6
190	60.8	58.0	2.8

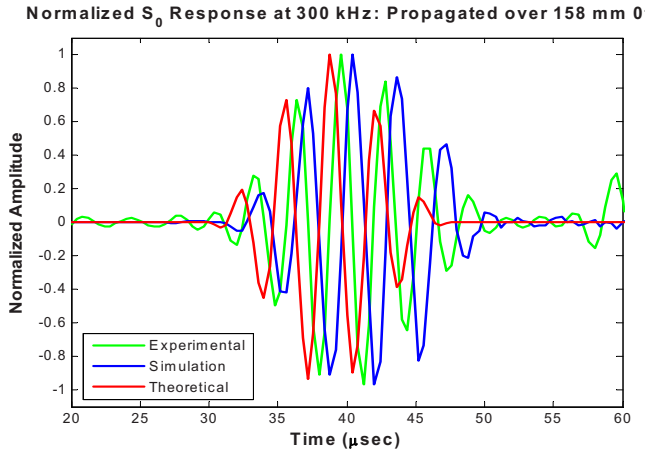

Fig. 16. Specimen I S_0 response at 300 kHz (0°F)

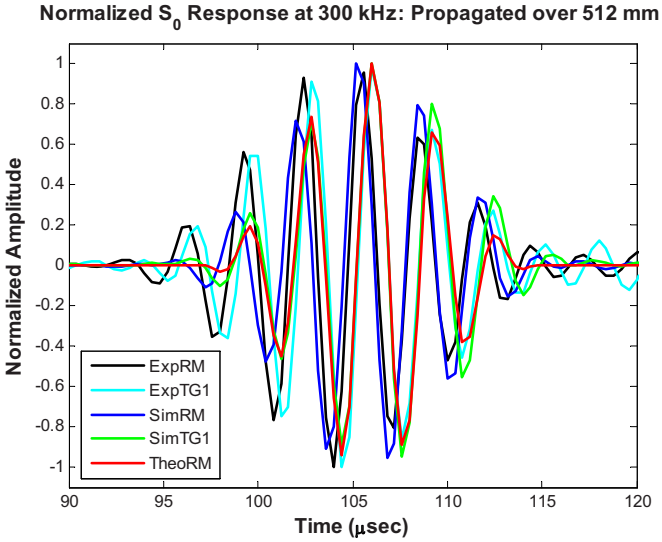

Fig. 17. Specimen III S_0 response comparison (RM versus TG 1) at 300 kHz

sponse and the large fluctuations after the S_0 response only explain small fluctuations after the S_0 response. Second, the magnetic noise that is introduced into the excitation signal needs to be considered in order to explain the fluctuations in this analysis. As mentioned before, the magnetic noise is a weakened excitation signal which is generated at the sensor. After the magnetic noise is generated, it is propagated to the circumference of the sensor. The small fluctuations before the S_0 responses are explained by a residual effect after the magnetic noise is propagated since the noise does not sufficiently damp out.

The large fluctuations after the S_0 responses can be explained by the interaction between two reflected waves in the signal that contains the magnetic noise. As shown in the figures, the wave propagates 158 mm (length of the wave path) for 30 μs. Since the magnetic noise, which propagates into the x and z directions of the sensor (see Fig. 6 for directions), is reflected by the boundary of Specimen I, it returns to the sensor. The reflected magnetic noise is captured by the sensor around 54 and 42 μs because it travels about 320 and 248 mm, respectively. Interaction of these two reflected waves appears as noise in the response signal. Arrival time calculation can be easily verified.

Thermal Gradient Testing of Specimen III

The thermal gradient condition is analyzed using Specimen III. The analysis focuses on the delayed TOA that is due to the elevated temperature region between the actuator and the sensor. The thermal stress effects on the TOA and the waveform are also considered.

S_0 Response Comparison

In this section, the three types of S_0 responses are compared under the three thermal gradient conditions (i.e., TG 1, TG 2, TG 3) and room temperature (RM). For this analysis, the 300 kHz excitation signal is used to generate the response. The first, second, and third types of S_0 responses are the simulated response, the theoretical response, and the experimental response, respectively. One should note that the theoretical equations are only capable of considering an isothermal environment. Thus, only room temperature theoretical response is evaluated for comparison.

Figs. 17 and 18 show the visual waveform comparison between the three types of S_0 responses for each step of thermal gradient condition. Table 8 shows the TOA differences between the three types of S_0 responses. Before a comparison of the waveform and the TOA are performed, each of the three types of S_0 responses are normalized with respect to its own absolute maximum amplitude, then the time delays between simulated, theoretical, and experimental excitation signals are plotted.

Unlike the previous results, the theoretical S_0 responses are a little bit slower than experimental and simulated S_0 responses. However, when comparison of the simulated S_0 responses and theoretical S_0 responses are performed, they still show a close TOA. The small TOA differences are due to the different analyzing abilities between ABAQUS and Matlab. Also, the simulated

Table 7. Specimen I TOA of S_0 Response at 300 kHz

	Time of arrival (TOA)			TOA difference	
Temperature (°F)	Simulation TOA (μs)	Experimental TOA (μs)	Theoretical TOA (μs)	Sim—exp (μs)	Sim—theo (μs)
0	40.4	39.6	38.8	0.8	1.6
50	40.4	39.6	38.8	0.8	1.6
100	40.4	40.4	39.2	0.0	1.2
125	40.8	40.4	39.2	0.4	1.6
150	40.8	40.8	39.6	0.0	1.2
175	41.2	40.8	39.6	0.4	1.6
190	41.2	40.8	39.6	0.4	1.6

J. Aerosp. Eng., 2009, 22(2): 185-197

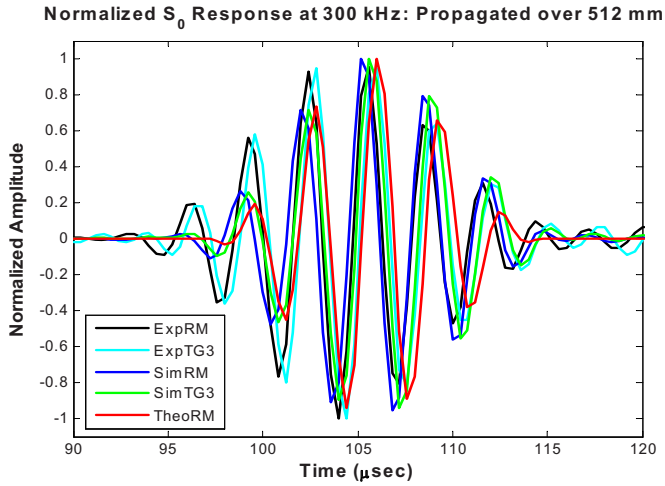

Fig. 18. Specimen III S_0 response comparison (RM versus TG 3) at 300 kHz

and experimental S_0 responses are delayed by a small amount as the temperature of the thermal gradient region increases. This phenomenon is similar to the isothermal condition, however, when we consider the specific condition of the thermal gradient (i.e., thermal stress exists along the wave path) the particular changes of the waveform and the large amount of TOA difference are not observed. It is shown that the effect of the thermal stress does not significantly change the wave propagation analysis. In addition, like previous responses, magnetic noise and other differences are observed between the results. Most of the differences can be explained by using the same reasons which are discussed in the previous section.

Summary and Conclusions

The objective of this investigation is to evaluate Lamb wave propagation through an aluminum plate considering various excitation signal pulse rates incorporated into the finite-element code ABAQUS CAE. These simulated results are compared to the theoretical predictions and experimental results under isothermal and thermal gradient conditions. To assess the sensitivity of the S_0 responses, the waveform and the TOA are determined.

In order to accomplish the objectives, the isothermal ABAQUS simulation is conducted under nine temperature (0, 25, 50, 75, 100, 125, 150, 175, and 190°F) and two frequency (100 and 300 kHz) conditions. The thermal gradient ABAQUS simulation is conducted under three thermal gradients and one frequency (300 kHz) condition. In all wave propagation analysis, it is apparent that the wave speeds are reduced by the increased temperature. As mentioned previously, these phenomena can be explained by the relations between the elastic modulus and the temperature of the material.

Similar waveforms and close TOA between the simulated, theoretical, and experimental results are enough to verify the ABAQUS simulation results in Lamb wave analysis. However, some differences between these results are also observed. These differences are assumed to be affected by the noise that is brought by the experimental setting. The experimental results include not only the responses that we want to measure but also noise that is generated in a real experiment. For precise analysis, this noise needs to be distinguished and explained. In this sense, ABAQUS can provide important criteria for distinguishing this noise from the pure results because the ABAQUS results include all effects (i.e., combination of the various Lamb wave modes and reflected Lamb waves) that occur during the analysis except for the noise that is related to the experiment. ABAQUS cannot distinguish between the Lamb wave modes and reflected waves from the boundaries. The Matlab program is used since it provides every single Lamb wave mode for a specific time. The experiment verifies the theoretical appropriateness of the simulation.

Small fluctuations, which are observed after the simulated S_0 responses, are explained by the differences between the simulated/experimental excitation signal and the theoretical excitation signal. Each simulated/experimental excitation signal has some noise after its 5 1/2 cycle Hanning-window excitation pulse. This noise can explain the small fluctuations after the S_0 responses in the simulated and experimental results. In addition, some small and large fluctuations are observed before and after the experimental S_0 responses which can be explained by the magnetic induction creating noise in the response signal. The small fluctuations before the S_0 responses are explained by the

Table 8. Specimen III TOA of S_0 Response

		Time of arrival (TOA)			TOA difference	
		Simulation TOA (μs)	Experimental TOA (μs)	Theoretical TOA (μs)	Sim—exp (μs)	Sim—theo (μs)
200 kHz	RM	109.2	106.4	110.8	2.8	−1.6
	TG 1	110.0	107.2	—	2.8	—
	TG 2	110.0	106.8	—	3.2	—
	TG 3	109.6	106.8	—	2.8	—
300 kHz	RM	105.6	105.6	106.0	0.0	−0.4
	TG 1	106.0	106.0	—	0.0	—
	TG 2	106.0	106.0	—	0.0	—
	TG 3	106.0	106.0	—	0.0	—
500 kHz	RM	101.2	100.8	102.4	0.4	−1.2
	TG 1	102.0	101.2	—	0.8	—
	TG 2	102.0	101.2	—	0.8	—
	TG 3	101.6	101.2	—	0.4	—

residual effect after the magnetic noise propagates since it does not sufficiently damp out. The large fluctuations after the S_0 responses are explained by the interaction between two reflected waves containing the magnetic noise. To generate more ideal responses, the wave absorbability that occurs through the supports and the air boundary conditions in the experiment needs to be modeled in the simulation and additional efforts to reduce the noise in the experimental responses are needed.

The wave propagation analysis is conducted after the thermal gradients reach steady-state condition, then the thermal stress field is evaluated. However, any significant changes, due to the effect of the thermal stress, in the waveform and TOA of the response, are not observed. This is due to the low stress value ($-0.176\ \mathrm{N/mm^2}$ in which the analysis is not presented) of the steady-state thermal stress field. Since only the steady-state thermal stress field is used, because of the sensitivity of the wave, it is difficult to observe any effects the thermal stresses have on wave propagation. Obviously, if high stress is used for the wave analysis, it will cause deformation and displacement on the specimen and alter the Lamb wave propagation analysis.

Acknowledgments

The writers would like to acknowledge M. Derriso AFRL-VA for his financial support and S. Olsen and M. DeSimio for their technical assistance. The views expressed in this work are those of the writers and do not reflect the official policy or position of the U.S. Air Force, the Department of Defense, or the United States Government. This material is declared a work of the United States Government and is not subject to copyright protection in the United States.

References

ABAQUS Inc. (2006). *Analysis user's manual, Version 6.6*, Providence, R.I.

Achenbach, J. D. (1980). *Wave propagation in elastic solids*, North-Holland, Amsterdam, The Netherlands.

Alleyne, D., and Cawley, P. (1991). "A two-dimensional Fourier transform method for the measurement propagating multimode signals." *J. Acoust. Soc. Am.*, 89(3), 1159–1168.

Andrews, J. (2007). "Lamb wave propagation in varying thermal environments." MS thesis, Air Force Institute of Technology (AU), Wright Patterson AFB, Ohio.

Cawley, P., and Alleyne, D. (1996). "The use of Lamb waves for the long range inspection of large structures." *Ultrasonics*, 34, 287–290.

Department of Defense. (2003). *Metallic materials and elements for aerospace vehicle structures*, MIL-HDBK-5J, Washington, D.C.

Derriso, M. M., Olson, S. E., DeSimio, M. P., and Sanders, B. (2005). "Development of automated damage detection techniques." *Materials damage prognosis*, J. M. Larson et al., eds., TMS, Warrendale, Pa.

Ghosh, T., Kundu, T., and Karpur, P. (1998). "Efficient use of Lamb modes for detecting defects in large plates." *Ultrasonics*, 36, 791–801.

Giurgiutiu, V. (2005). "Tuned Lamb wave excitation and detection with piezoelectric wafer active sensors for structural health monitoring." *J. Intell. Mater. Syst. Struct.*, 16(4), 291–305.

Grisso, B. L. (2004). "Considerations of the impedance method, wave propagation, and wireless systems for structural health monitoring." Master's thesis, Virginia Polytechnic Institute and State Univ., Blacksburg, Va.

Han, S. (2007). "Finite element analysis of Lamb wave propagation in a thin aluminum plate." MS thesis, Air Force Institute of Technology (AU), Wright Patterson AFB, Ohio.

Kundu, T., Maji, A., Gosh, T., and Maslov, K. (1998). "Detection of kissing bonds by Lamb waves." *Ultrasonics*, 35, 573–580.

Kundu, T., Maslov, K., Karpur, P., Matikas, T. E., and Nicolau, P. D. (1996). "A Lamb wave scanning approach for the mapping of defects in [0/90] titanium composites." *Ultrasonics*, 34, 43–49.

Lamb, H. (1917). "On waves in an elastic plate." *Proc. R. Soc. London, Ser. A*, 93(648), 114–128.

Lathi, B. P. (2005). *Linear systems and signals*, Oxford University Press, Oxford, N.Y., 16–17.

Lempriere, B. M. (2002). *Ultrasound and elastic waves*, Academic, New York.

Lowe, M. J. S., Alleyne, D. N., and Cawley, P. (1998). "Defect detection in pipes using guided waves." *Ultrasonics*, 36, 147–154.

Mal, A. (2004). "Structural health monitoring." *The American Academy of Mechanics Bi-monthly Newsletter*, "*Mechanics*," 33(11–12), 1–4.

Moser, F., Jacobs, L. J., and Qu, J. (1999). "Modeling elastic wave propagation in waveguides with the finite element method." *NDT & E Int.*, 32(4), 225–234.

Olson, S. E., Derriso, M. M., DeSimio, M. P., and Thomas, D. T. (2006). "Analytical modeling of Lamb waves for structural health monitoring." *Proc., 3rd European Workshop on Structural Health Monitoring*, Granada, Spain.

Rose, J. L. (1999). *Ultrasonic waves in solid media*, Cambridge University Press, Cambridge, Mass.

Saada, A. S. (1993). *Elasticity theory and applications*, Krieger, Malabar, Fla.

Timoshenko, S., and Goodier, J. (1970). *Theory of elasticity*, McGraw-Hill, New York, 433–441.

Wait, J. R., Park, G., and Charles, R. F. (2005). "Integrated structural health assessment using piezoelectric active sensors." *Shock Vib.*, 12, 389–405.

Worlton, D. C. (1957). "Ultrasonic testing with Lamb waves." *Nondestr. Test. (Chicago)*, 15, 218–222.